Attention as Robust Representation for Time Series Forecasting

PeiSong Niu [*1] **Tian Zhou** [*1] **Xue Wang** [1] **Liang Sun** [1] **Rong Jin** [1 2]

Abstract

Time series forecasting is essential for many practical applications, with the adoption of transformer-based models on the rise due to their impressive performance in NLP and CV. Transformers' key feature, the attention mechanism, dynamically fusing embeddings to enhance data representation, often relegating attention weights to a byproduct role. Yet, time series data, characterized by noise and non-stationarity, poses significant forecasting challenges. Our approach elevates attention weights as the primary representation for time series, capitalizing on the temporal relationships among data points to improve forecasting accuracy. Our study shows that an attention map, structured using global landmarks and local windows, acts as a robust kernel representation for data points, withstanding noise and shifts in distribution. Our method outperforms state-of-the-art models, reducing mean squared error (MSE) in multivariate time series forecasting by a notable 3.6% without altering the core neural network architecture. It serves as a versatile component that can readily replace recent patching based embedding schemes in transformer-based models, boosting their performance. The source code for our work is available at: `https://anonymous.4open.science/r/AttnEmbed-7430`.

1. Introduction

Time series forecasting is a vital problem that has played an important role in many real-world applications (Wen et al., 2022; Courty & Li, 1999; Böse et al., 2017; Li et al., 2019), ranging from energy, weather, traffic to economics. In recent years, traditional statistical and machine learning methods (Box & Jenkins, 1968; Box & Pierce, 1970) have been gradually replaced by deep learning models in time series forecasting. In particular, CNN and MLP-based models (Wu et al., 2023; Zeng et al., 2023) have shown great performance improvement in time series analysis. Moreover, following the successes in NLP (Vaswani & etc., 2017; Devlin et al., 2019; Radford et al., 2019) and CV (Dosovitskiy et al., 2021; Bao et al., 2022), transformer models (Wen et al., 2023; Zhou et al., 2021; Wu et al., 2021; Zhou et al., 2022b; Nie et al., 2022; Liu et al., 2023; Xue et al., 2023) have demonstrated impressive results. Among the transformer models, PatchTST (Nie et al., 2022) successfully applies the idea of vision transformer (ViT) (Dosovitskiy et al., 2021) to time series by segmenting the time series into multiple patches to serve as input tokens for transformers. While segmentation is beneficial for reducing information redundancy, it overlooks the relationship between a time point and its neighbors, making it insufficient for noise reduction and to handle rapid distribution drifts.

The attention mechanism is a pivotal component that underpins the transformative success of the transformer model across various domains. It is widely regarded as the linchpin behind monumental advancements such as ChatGPT and Midjourney, although other elements like feed-forward networks (FFNs) and positional embeddings also play significant roles. Essentially, the attention mechanism functions as a dynamic, weighted feed-forward layer. Within a self-attention layer, for instance, queries (Q) and keys (K) are used to calculate an attention matrix, which subsequently serves as a weighting matrix that synthesizes the values (V). The resultant attention matrix is usually viewed as a byproduct to reveal the quantitative influence of each input token and to effectively aggregate information across different tokens.

Although time series forecasting can be naturally viewed as a sequence modeling problem, it differs significantly from token sequences in CV or NLP in which limited information can be founded in patches because every data point in time series is simply a scalar. In contrast, tokens in both CV and NLP encompass significantly richer information in that we often find considerable amount of redundant information across different tokens, evidenced by high masking rates used in self supervised learning in CV and NLP. Furthermore, many time series data often contain noises and distribution shifts, partly due to high sampling rates (Wen et al.,

[*]Equal contribution [1]Alibaba Group [2]The author now works at Meta Platforms, Inc. Correspondence to: Tian Zhou <tian.zt@alibaba-inc.com>, Rong Jin <rongjinemail@gmail.com>.

2022), making the forecasting more challenging. These observations inspire us to develop a richer and robust representation for time series data. Since weights in the attention matrix reveal the pairwise relationship between different patches in time series, motivated by the theory of kernel learning (Wilson et al., 2015) and reproduced kernel Hilbert space (Ghojogh et al., 2021), we propose a novel and robust data representation based on the attention matrix that captures the relationship among different data points in the same time series. One obvious advantage of using attention weights for data representation is that it helps capture the overall seasonality of time series, a special complex relationship. In Section 2.2 and Appendix A, we demonstrate that, based on kernel learning theory, employing attention weights as representations more effectively captures the intricate relationships among data points.

We also note previous efforts that connect attention mechanism with kernel function. For instance, several studies (Tsai et al., 2019; Katharopoulos et al., 2020; Song et al., 2021) have explored attention from the perspective of kernel functions, either to propose a new paradigm for transformers or to reduce the computational complexity. In addition, (Mika et al., 1998) exploited non-linear kernel functions to reduce noise in time series while preserving the relationship between different time points. In this study, we also show that using kernel functions, such as polynomial kernels, in attention matrix computation can be more effective for time series forecasting than the standard softmax.

Several studies have leveraged the attention matrix's pairwise relationships for time series anomaly detection. For example, Anomaly Transformer (Xu et al., 2021) introduces an association discrepancy by measuring the Kullback-Leibler divergence between the attention matrix and a learnable Gaussian kernel to identify anomalies. Similarly, DCdetector (Yang et al., 2023) suggests that the divergence between attention matrices is a dependable indicator. However, our work is not limited by the anomaly detection framework. Instead, we have developed a generalized data representation from the attention matrix, which presents versatile potential for tasks involving embeddings.

Our contributions in this paper are summarized as follows:

- Attention as robust representation: We propose a novel time series representation method called AttnEmbed, which utilizes attention weights as representation of time segments. The resilience of AttnEmbed to both noise and non-stationary distributions is verified by our empirical studies of synthetic datasets, and is also verified by our theoretical analysis.
- Outstanding performance for time series forecasting: Our innovative embedding schema, AttnEmbed, integrates a global landscape and smoothing design to adeptly handle distribution shifts. When paired with a vanilla transformer, this approach significantly outperforms state-of-the-art methods in time series forecasting, as evidenced by our comprehensive experimental analysis.
- Kernel functions for better attention: We illustrate that the polynomial kernel can effectively replace traditional similarity measures in attention mechanisms, yielding representations that enhance performance in forecasting tasks.
- General plug-in: AttnEmbed can be seamlessly integrated as a general plug-in module. We have effectively integrated it into multiple methods, yielding performance enhancements over the patching method.

2. Attention as Robust Representation

To verify the resilience of attention as a data representation to both noise and non-stationary distributions, we first conduct experiments on synthetic data, and then examine the robustness of attention based representation by a theoretical analysis.

2.1. An Empirical Study on Synthetic Data

We develop two synthetic datasets, one for non-stationary time series and one for noisy data, and compare our approach (i.e. AttnEmbed), against a method that inputs patches of the original data with linear projection for embedding (i.e., PatchTST,VIT).

Synthetic Data. The synthetic data is generated by the aggregation of 10 sinusoids and cubic functions, each characterized by distinct random parameters:

$$f_1(x) = \sum Asin(\omega x + \phi) + \sum (ax^3 + bx^2 + cx + d),$$
$$f_2(x) = \sum Asin(\omega x + \phi) + \sum (ax^3 + bx^2 + cx + d) + \sigma,$$

where $f_1(x)$ is a designed for non-stationary distribution and $f_2(x)$ is designed for noisy data. All the parameters in $f_1(\cdot)$ and $f_2(\cdot)$ are randomly chosen. A total of 2000 time steps are sampled, with a lookback window size of 192 and the forecast horizon of 96. Figure 1 shows the plots of the two functions, together with all experimental results for comparison.

Non-stationary Data. Figure 1 (a) shows time series data generated by $f_1(\cdot)$, which clearly show a noticeable shift. We can observe that the proposed representation AttnEmbed is able to better capture the overall drift than PatchTST for the first 50 time points of forecasting, and the advantage disappears after time point 250.

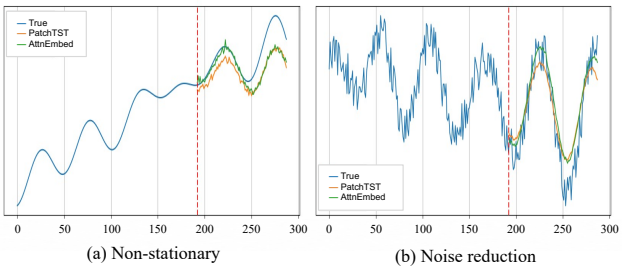

(a) Non-stationary (b) Noise reduction

Figure 1. Comparison between AttnEmbed (ours) and PatchTST on synthetic data. (a) Non-stationary. (b) Noise reduction.

Noise Reduction. Figure 1 (b) shows the time series generated by $f_2(\cdot)$ (i.e. $f_1(\cdot)$ plus noise). Experimental results indicate that while both AttnEmbed and PatchTST effectively mitigate noise, AttnEmbed delivers more accurate predictions for imminent time points in forecasting.

In conclusion, our empirical studies using synthetic data demonstrate that attention-based embedding is an effective schema for addressing noise and non-stationary distributions.

2.2. Theoretical Analysis for Robustness of Attention based Representation

To demonstrate that AttnEmbed is more resilient to noise, we first will show that by adding significant amount of noises to the input patterns, the distance of "similar" data pairs can be very close to that for "dissimilar" pairs. In constrast, by using attention based representations, we are able to maintain that the distance for "similar" data pairs is significantly smaller than that for "dissimilar" pairs even after adding large noises to the input patterns. Below, we will provide the sketch of overall results, and postpone the full analysis to the appendix.

Consider we have n vectors $x_i \in \mathbb{R}^d$ in a sequence that are generated from $m < d$ Gaussian distributions $\mathcal{N}(\mu_i, I_d), i = 1, \ldots, m$. We assume $\langle \mu_i, \mu_j \rangle = \delta_{i,j} s$. It is easy to show that for two "similar" data points x_i^+ and x_j^+ that are generated from the same distribution, their expected distance is $\mathrm{E}[|x_i^+ - x_j^+|^2] = 2d$, whereas for two "dissimilar" data points x_i^- and x_j^+ that are generated from different distributions, their expected distance is $\mathrm{E}[|x_i^- - x_j^-|^2] = 2d + 2s$. When $s \ll d$, i.e., noises are much larger than signals, we have $\mathrm{E}[|x_i^+ - x_j^+|^2] \approx \mathrm{E}[|x_i^- - x_j^-|^2]$, implying that there is a significant chance that $|x_i^- - x_j^-|^2$ can be noticeably smaller than $|x_i^+ - x_j^+|^2$. Now, if we use the attention weights as the representation, denoted by $f(x)$, using the same notation for "similar" and "dissimilar" data pairs, we can show that

$$\frac{\mathrm{E}[|f(x_i^-) - f(x_j^-)|^2] - \mathrm{E}[|f(x_i^+) - f(x_j^+)|^2]}{|f(x_i^-) - f(x_j^-)|^2] = \Omega(1)}$$

with appropriate choice of temperature. It implies that even after adding large noises to input patters, we can still clearly distinguish "similar" data pairs from the "dissimilar" data pairs, thus verifying the robustness of the proposed attention based data representation. The full theoretical analysis is in appendix A.

3. Related Work

In this section, we provide brief reviews of literature in the areas of time series forecasting and the relationship between attention mechanism and kernel function.

3.1. Time Series Forecasting

Recently, inspired by great success in NLP and CV, transformer models have also been widely used in time series forecasting (Wen et al., 2023). Informer (Zhou et al., 2021) proposes a probability sparse attention mechanism to deal with long-term dependencies. Autoformer (Wu et al., 2021) introduces a decomposition transformer architecture and replaces the attention module with an Auto-Correlation mechanism. FEDformer (Zhou et al., 2022b) employs a Fourier-enhanced architecture to improve computational efficiency, achieving linear complexity. PatchTST (Nie et al., 2022) segments time series into individual patches, which successfully increases input length and reduce information redundancy. GPT4TS (Zhou et al., 2023) utilizes a frozen GPT-2 and achieves a promising performance in several time series tasks. CARD (Xue et al., 2023) and iTransformer (Liu et al., 2023) integrates the correlations among multiple variables to enhance the performance in multivariate time series forecasting. Moreover, TimesNet (Wu et al., 2023) treats time series as a 2D signal and utilizes a convolution-based inception network as its backbone. A simple MLP-based DLinear (Zeng et al., 2023) outperforms a lot of transformer models in time series forecasting with channel-independence and seasonal-trend decomposition.

3.2. Attention and Kernel Function

The perspective of viewing attention as a kernel function is widely recognized in the literature, encompassing modifications to transformers and attention mechanisms (Tsai et al., 2019; Song et al., 2021), acceleration of computational processes (Katharopoulos et al., 2020), and time series anomaly detection (Yang et al., 2023; Xu et al., 2021). (Tsai et al., 2019) proposes that the attention mechanisms in transformers can be interpreted as employing a kernel smoother across the input data and the kernel scores is the similarities between inputs. (Song et al., 2021) derives that the attention is a product of RBF kernel and the exponential of ℓ_2-norm. Also, given kernel functions are advantageous in computational efficiency for distance calculations, (Katharopoulos et al., 2020) reformulates self-attention as a linear operation

involving the dot-product of kernelized feature maps. Excitingly, the exploration of kernel functions has extended into the realm of time series anomaly detection. Anomaly Transformer (Xu et al., 2021) and DCDetector (Yang et al., 2023) both utilize Kullback-Leibler divergence to calculate the distance between attention matrix and Gaussian kernel, establishing a novel linkage between attention mechanisms and kernel functions in the domain of time series. Although the methods mentioned previously utilize attention weights primarily for token mixing, our work is among the first to explore attention as an end in itself—not just a means—for embedding schema in the field of time series forecasting. To our knowledge, such an approach has been rarely investigated.

4. Methodology

Consider a multivariate time series with look back window L: $(x_1, ..., x_t, ..., x_L)$, where $x_t \in \mathbb{R}^M$ is the observation at time t with M channels. Our objective is to forecast future steps with a horizon of T, denoted by $(x_{L+1}, ..., x_{L+T})$.

4.1. Overall Architecture

The architecture of AttnEmbed is illustrated in Figure 2. AttnEmbed contains Pre-processing module which consists of instance normalization and channel independence, Attention Embedding module and Transformer Encoder.It is important to note that our proposed method serves as a model-agnostic alternative for embedding, with the transformer employed merely as an illustrative example. As demonstrated in Table 7, we have conducted experiments with various baseline models, including PatchTST (Nie et al., 2022) and CARD (Xue et al., 2023).

Pre-process Module. The input time series in Pre-process module is first normalized by instance normalization (Kim et al., 2022). This normalization block performs a simple normalization of the input time series with mean and variance, and subsequently integrates these values back to the output. We then employ the channel independence technique, as used in DLinear (Zeng et al., 2023) and PatchTST (Nie et al., 2022), which has been widely validated for its effectiveness in time series forecasting. This technique essentially transforms a multivariate time series forecasting problem into a univariate one.

Attention Embedding Module. The Attention Embedding module is critical in the architecture of AttnEmbed. The pre-processed time series is split into multiple windows in the Attention Embedding module. Within each window, we utilize a shared Embedding self-attention block with L layers to extract the mutual relationships between time steps. Specifically, for each window, we extract the intermediary computational outputs generated by the Embedding module, obtaining a set of attention matrices. Then, all the last row of attention matrices are concatenated to form the embedding for the respective window.

Transformer Encoder. Similar to PatchTST (Nie et al., 2022), next we employ a Transformer Encoder based on the generated embeddings for the forecasting task. As shown in Figure 2, compared to PatchTST, the primary distinction is that AttnEmbed integrates the interaction between time steps within a single window or patch, which is essential for addressing distribution shift by capturing local dynamics.

4.2. Attention Embedding

We now delve into the specifics of computing the attention embedding, as depicted in Figure 5. The pre-processed univariate time series is represented as $U = [u_1, ..., u_t, ..., u_L] \in \mathbb{R}^L$, where L is the length of the series.

4.2.1. Tokenization and Global Landmark

Each input univariate time series is split into several overlapped or non-overlapped windows with window size W and stride length S. Thus, the raw tokens are generated as $\hat{\mathcal{X}} = [x_1^w, ..., x_i^w, ..., x_N^w] \in \mathbb{R}^{W \times 1 \times N}$, where $N = \lfloor \frac{L-W}{S} \rfloor + 1$. Each window, comprising W time steps, is processed through a common set of self-attention layers to yield a concatenated attention matrix, which is then utilized as the embedding.

While the above attention embedding method benefits from capturing local information, it overlooks the global information of the time series. Thus, we introduce global landmarks designed to incorporate the information from the entire series. We utilze Conv1D to calculate the global landmarks:

$$x_g^w = \text{Conv1D}(x_i^w), \tag{1}$$

where $x_g^w \in \mathbb{R}^G$ and G represents the number of landmarks, which is dictated by the parameters of Conv1D. Subsequently, the embedding matrix formed by the shared attention layers is assembled by concatenating each local feature representation x_t^w with the corresponding global feature representation x_g^w:

$$\mathcal{X} = [[x_g^w, x_1^w], ..., [x_g^w, x_N^w]], \tag{2}$$

where $\mathcal{X} \in \mathbb{R}^{(G+W) \times 1 \times N}$.

For each individual window, the attention score of the h-th head in the l-th layer is denoted as $A_h^l \in \mathbb{R}^{(G+W) \times (G+W)}$ Through the combination and projection of these attentions, an embedding can be generated that characterizes the local information of the window. Specifically, the final rows from all attention matrices are concatenated and subsequently

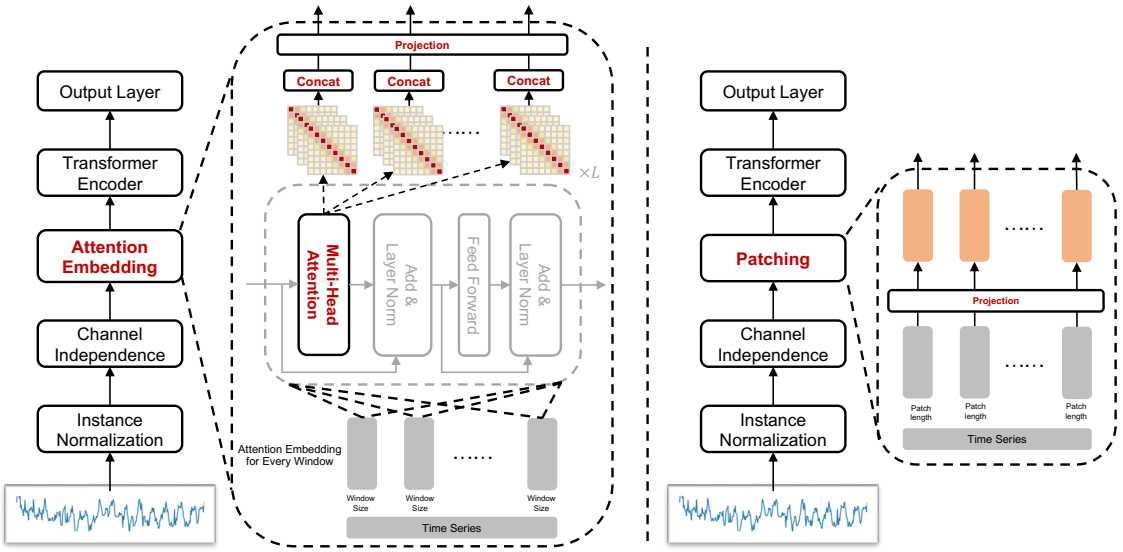

(a) AttnEmbed (b) PatchTST

Figure 2. The architecture of (a) AttnEmbed and a comparison with (b) PatchTST. Unlike PatchTST, AttnEmbed considers the relationship of time steps within each window.

passed through a projection layer:

$$x^{emb} = \text{Proj}(A^{cat}), \tag{3}$$

$$A^{cat} = \underset{L^a in[1,L^a],h\in[1,H^a]]}{\text{Concat}} (A_h^l[-1,:]), \tag{4}$$

where $A^{cat} \in \mathbb{R}^{L^a H^a (G+W)}$, L^a and H^a represent the number of layers and the number of heads in the set of self-attention layers of the embedding module respectively. Thus the final output embedding can be denoted as $\mathcal{X}^{emb} = [x_1^{emb}, ..., x_N^{emb}]$.

4.2.2. Exponential Moving Average (EMA)

To enhance the capture of local information, we have incorporated an Exponential Moving Average (EMA) within the self-attention blocks of the embedding module. EMA is a special case of moving average that responds to changes more quickly in time and can smooth out the output for noise reduction. Specifically, EMA utilizes factors exponentially decaying weighting factors as:

$$y_t = \alpha x_t + (1-\alpha) y_{t-1}, \tag{5}$$

where $\alpha \in (0,1)$ is the degree of weighting decrease. Many works (Ma et al., 2023; Xue et al., 2023) have explored the application of EMA in the attention module. We integrate EMA into the queries and keys within the attention mechanism, opting for a non-parametric approach to reinforce stability during the training process.

4.3. Kernel Function for Attention based Representation

Inspired by earlier studies (Choromanski et al., 2021; Katharopoulos et al., 2020) that pioneered a kernel-based interpretation of the attention matrix, we propose the adoption of advanced kernel methods. We utilize both the Radial Basis Function (RBF) and polynomial kernels to assess the degree of similarity between time steps within a given window. This methodological innovation underpins the output of our attention embedding module, thereby replacing the $\mathcal{X}^{emb}$ as described in Section 4.2.

We generate queries Q and keys K by linearly projecting the token tensor $\mathcal{X}_i = [x_g^w, x_i^w]^T \in \mathbb{R}^{(G+W)\times 1}$ as follows:

$$Q = F_q(\mathcal{X}i), \quad K = F_k(\mathcal{X}i), \tag{6}$$

with both $Q, K \in \mathbb{R}^{(G+W)\times d}$, where F_q, F_k map from dimension 1 to d through MLP layers. These matrices are further processed to obtain $Q_h, K_h \in \mathbb{R}^{(G+W)\times dhead}$, corresponding to the queries and keys for the h^{th} attention head, with $d = H_a \times dhead$.

Kernel-based embeddings are then computed as:

$$x_{kernel}^{emb} = Proj(A_{kernel}^{cat}), \tag{7}$$

$$A_{kernel}^{cat} = \underset{h\in[1,H^a]}{\text{Concat}} \mathcal{K}(Q_h[-1,:], K_h), \tag{8}$$

where $\mathcal{K}$ is the kernel function. In this paper, we introduce two kernel functions, the RBF kernel and the polynomial kernel.

5. Experiments

5.1. Experiments on Real-world Datasets

Datasets. We conduct experiments on seven popular real-world benchmark datasets, including 4 ETT dataset (Zhou

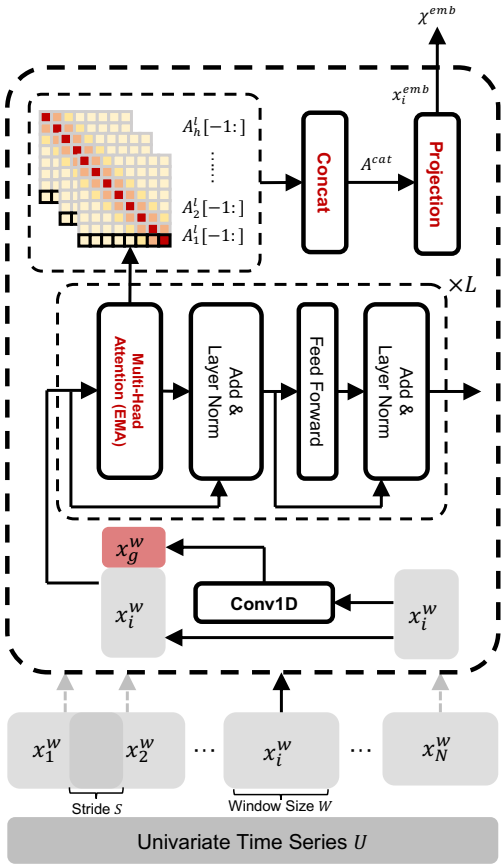

Figure 3. Detail of attention embedding.

et al., 2021) (comprising of two hourly dayasets ETTh1, ETTh2 and two 15-minute datasets ETTm1, ETTm2), the Electricity [1] dataset for hourly electricity consumption, the Weather [2] dataset for 10-minute weather forecasting and the Traffic [3] dataset for hourly road occupancy rate.

Baselines. In our comparison, we have chosen a range of representative baselines, including transformer-based models such as PatchTST (Nie et al., 2022), FiLM (Zhou et al., 2022a), FEDformer (Zhou et al., 2022b), Autoformer (Wu et al., 2021), and Informer (Zhou et al., 2021); the MLP-based DLinear (Zeng et al., 2023); and the CNN-based TimesNet (Wu et al., 2023). Our research is particularly concerned with exploring interactions within individual channels, so we've limited our benchmarking to cutting-edge models that adopt a channel-independent structure. This selection criterion ensures a focused and pertinent benchmarking against our research aims. Consequently, models like iTransformer (Liu et al., 2023) and CARD (Xue et al., 2023) are excluded from the primary experiments. Nonetheless, in Section 5.1.2, we demonstrate how AttnEmbed can be effectively integrated as a plug-in to enhance CARD's performance.

[1]https://archive.ics.uci.edu/ml/datasets/ElectricityLoadDiagrams20112014

[2]https://www.bgc-jena.mpg.de/wetter/

[3]http://pems.dot.ca.gov

Main Results. For better comparison, we follow the experimental settings in (Wu et al., 2023), maintaining the lookback length at 96, and the horizon length at 96, 192, 336, and 720, respectively. The main results of multivariate forecasting are summarized in Table 5. The lower MSE/MAE indicates the better forecasting results. AttnEmbed notably achieves state-of-the-art results, outshining the top-performing PatchTST model. Crucially, this is achieved while preserving a similar main model architecture, specifically the vanilla transformer encoder used by PatchTST. The enhancement in performance can be solely attributed to our shift from traditional patching to the AttnEmbed method, marking this advancement as substantial. AttnEmbed gains the best performance on 6 out of 7 datasets in both MSE and MAE. Compared with PatchTST, AttnEmbed yield an overall 3.6% relative MSE reduction and 2.1% relative MAE reduction. In datasets with noisier and more frequently shifting distributions, such as ETTh1 and Traffic, the improvement from PatchTST to AttnEmbed is more pronounced, achieving a significant reduction in MSE by 6.2% and 8.2%, respectively. In general, the improvements made by AttnEmbed are consistent across various horizons, indicating that attention effectively represents time series with the resilience of both noise and non-stationary distributions.

Recent works have shown that extending the lookback length can enhance performance. Thus, we have also demonstrated that AttnEmbed's effectiveness is not constrained by the lookback window size and can outperform PatchTST with longer inputs, in Section 5.1.2.

5.1.1. Kernel Functions

Our experiments with real-world datasets (ETTh1, ETTm1, and Weather) using RBF and polynomial kernels demonstrate that kernel functions can achieve results comparable to softmax-based attention mechanisms. The summarized outcomes in Table 6 indicate that both kernels not only meet but, on average, surpass the performance of previous state-of-the-art (SOTA) models like PatchTST and TimesNet in terms of MSE and MAE. Impressively, the polynomial kernel attains a relative MSE reduction of 4.2% and MASE reduction of 2.0% compared to PatchTST on ETTh1. These findings suggest that the effectiveness of attention weights can be replicated through a kernel approach, where similarities between tokens are calculated. Consequently, this validates the integration of kernel functions into time series forecasting, underscoring their viability and promising potential for such applications.

Table 1. Multivariate forecasting with a lookback length of 96. All models are averaged from 4 different horizons. A lower MSE indicates better performance. The best ones are in Bold, and the second ones are underlined. Detailed results are provided in Appendix B.1

Methods	**AttnEmbed**		PatchTST		TimesNet		DLinear		FiLM		FEDformer		Autoformer		Informer	
Metric	MSE	MAE	MSE	MAE	MSE	MAE	MSE	MAE	MSE	MAE	MSE	MAE	MSE	MAE	MSE	MAE
Weather	**0.252**	**0.278**	0.257	0.280	0.259	0.287	0.265	0.317	0.269	0.339	0.309	0.360	0.338	0.382	0.634	0.548
ETTh1	**0.422**	**0.430**	0.450	0.440	0.458	0.450	0.456	0.452	0.461	0.456	0.440	0.460	0.496	0.487	1.040	0.795
ETTh2	**0.361**	**0.393**	0.366	0.404	0.414	0.427	0.559	0.515	0.384	0.406	0.437	0.449	0.450	0.459	4.431	1.729
ETTm1	**0.377**	**0.395**	0.381	**0.395**	0.400	0.406	0.403	0.407	0.408	0.399	0.448	0.452	0.588	0.517	0.961	0.734
ETTm2	0.286	0.331	**0.285**	**0.327**	0.291	0.333	0.350	0.401	0.287	0.328	0.305	0.349	0.327	0.371	1.410	0.810
ECL	**0.189**	**0.274**	0.196	0.280	0.192	0.295	0.212	0.300	0.223	0.303	0.214	0.327	0.227	0.338	0.311	0.397
Traffic	**0.447**	**0.282**	0.487	0.308	0.620	0.336	0.625	0.383	0.639	0.389	0.610	0.376	0.628	0.379	0.311	0.397

Table 2. Multivairate forecasting results with RBF kernel and polynomial kernel with a lookback length of 96. All models are averaged from on 4 different horizons. A lower MSE indicates better performance. The best ones are in Bold, and the second ones are underlined. Detailed results are provided in Appendix B.2

Methods	AttnEmbed		RBF Kernel		Polynomial Kernel		PatchTST		TimesNet	
Metric	MSE	MAE	MSE	MAE	MSE	MAE	MSE	MAE	MSE	MAE
Weather	**0.252**	**0.278**	0.255	0.280	0.254	0.279	0.257	0.280	0.259	0.287
ETTh1	**0.422**	**0.430**	0.445	0.439	0.431	0.431	0.450	0.440	0.458	0.450
ETTm1	**0.377**	0.395	0.378	**0.393**	0.379	**0.393**	0.381	0.395	0.400	0.406

Table 3. Utilize AttnEmbed as a plug-in. The lookback length is 336 for PatchTST and 96 for CARD. All models are averaged from 4 different horizons. A lower MSE indicates better performance. Detailed results are provided in Appendix B.3.

Methods	PatchTST(42)		PatchTST(42) +AttnEmbed		CARD		CARD +AttnEmbed	
Metric	MSE	MAE	MSE	MAE	MSE	MAE	MSE	MAE
Weather	0.229	0.265	**0.227**	**0.263**	0.239	0.265	**0.238**	**0.260**
ETTh1	0.417	0.430	**0.409**	**0.426**	0.442	0.428	**0.436**	**0.427**
ETTh2	0.352	0.381	**0.347**	**0.379**	0.383	0.384	**0.377**	**0.379**

5.1.2. Utilize AttnEmbed as a Plug-in

As depicted in Figure 5, the primary distinction between AttnEmbed and PatchTST lies in the embedding module. Consequently, AttnEmbed could potentially serve as a plug-in module to replace patching. Here, we primarily investigate two aspects of AttnEmbed's versatility: the extension of the lookback window and the incorporation of multi-channel relationships. We have smoothly incorporated the AttnEmbed module into the PatchTST framework (42) with a lookback window of 336 time steps, and into the CARD model, which utilizes a 96-step lookback window and is tailored to improve cross-channel interactions. This strategic integration underscores the adaptability and strength of our design as a robust plug-in module, demonstrating its efficacy over diverse input horizons. To ensure a fair comparison, the window size, stride settings, and lookback window are kept in line with those used in the respective original models. The results are summarized in Table 7. After substituting the patching with AttnEmbed, we can observe a performance improvement even when retaining the same window size and stride. Notably, on the ETTh1 dataset, AttnEmbed achieves a relative MSE reduction of 1.9% when integrated with PatchTST(42), and a relative MSE reduction of 1.3% for CARD. This indicates that AttnEmbed is versatile beyond the constraints of lookback window and channel-independent settings, demonstrating its potential as an adaptable plug-in module for various models.

5.2. Model Analysis

5.2.1. Ablations

Here, we carry out ablation studies for the architectural design of AttnEmbed, with the aim of demonstrating the performance impact of omitting the global landmark or EMA components. Two ablated versions of AttnEmbed are evaluated on the ETTh1 and ETTm1 datasets: 1) AttnEmbed without global landmark, to assess the significance of incorporating global information; and 2) AttnEmbed without EMA, to ascertain the contribution of EMA to time series forecasting. As depicted in Table 8, the fully-equipped AttnEmbed model, which integrates both landmark and EMA, outperforms its two ablated variants by achieving an average MSE reduction of 2.2%. This highlights the crucial roles that landmarks and EMA play within the AttnEmbed framework, effectively capturing global information and local time-dependent dynamics.

Table 4. Ablation on EMA and landmark with a lookback length of 96. All models are averaged from 4 different horizons. A lower MSE indicates better performance. Detailed results are provided in Appendix B.4

Methods	AttnEmbed		AttnEmbed w/o EMA		AttnEmbed w/o Landmark	
Metric	MSE	MAE	MSE	MAE	MSE	MAE
ETTh1	0.422	0.430	0.432	0.427	0.423	0.429
ETTm1	0.377	0.395	0.384	0.397	0.386	0.397

5.2.2. Parameter Analysis

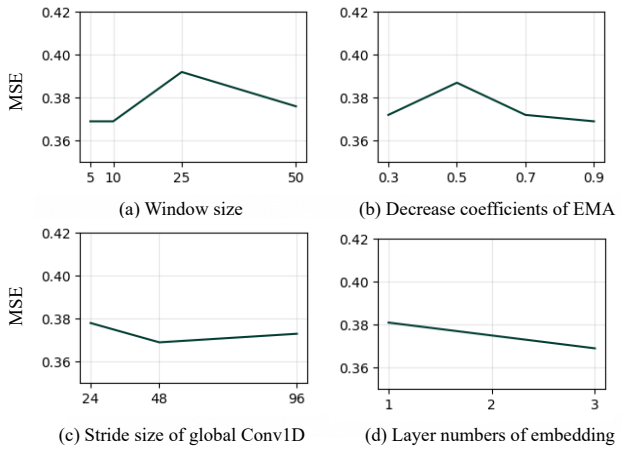

(a) Window size (b) Decrease coefficients of EMA

(c) Stride size of global Conv1D (d) Layer numbers of embedding

Figure 4. Parameter analysis on ETTh1 with a lookback window of 96 and a horizon of 96. (a) Window size. (b) Decrease coefficients of EMA. (c) Stride sizes of global Conv1D. (d) Layer numbers of the attention embedding module.

We examined AttnEmbed's parameter sensitivity, presenting the forecasting MSE for varying configurations in Figure 4. These parameters include window sizes ([5, 10, 25, 50]), EMA decay coefficients ([0.3, 0.5, 0.7, 0.9]), Conv1D stride sizes ([24, 48, 96]), and attention embedding module layers ([1, 2, 3]), all tested on the ETTh1 dataset with a 96-period lookback and forecast horizon.

Figure 4(a) reveals that larger window sizes struggle with quick distribution changes. In contrast, as shown in Figure 4(b), the proper EMA decay coefficient can enhance results and mitigate noise, although too low a coefficient may oversmooth and degrade performance. Figure 4(c) suggests that a stride size around half the lookback window optimizes the capture of global patterns. Lastly, Figure 4(d) indicates that deeper attention embedding layers improve outcomes, with three layers being selected for their balance of performance and computational efficiency.

5.2.3. Alleviating Rank Collapse

Rank collapse is a notable challenge in the application of transformer models, wherein the attention matrix's rank decreases during training. This contraction in rank can constrain the model's ability to fit data, leading to weaker generalization. Although this issue affects transformers for time series (TS), they are less prone to it compared to the more layered Large Language Models (LLMs), yet it remains a relevant concern for TS model robustness.Since attention matrix is closely related to kernel matrix that often exhibits a higher rank than the input matrix, we expect the introduction of attention based representation may help alleviate the problem of rank collapse.

Though following (Dong et al., 2021), we compare the relative norm of the residual to evaluate the 'rankness' of layers in a model. As shown in Figure 5, using the attention based representation, where pairwise similarities are computed using RBF and polynomial kernels, can efficiently mitigate the issue of rank collapse observed in time series data. More information about kernel function for attention based representation can be found in Section 4.3.

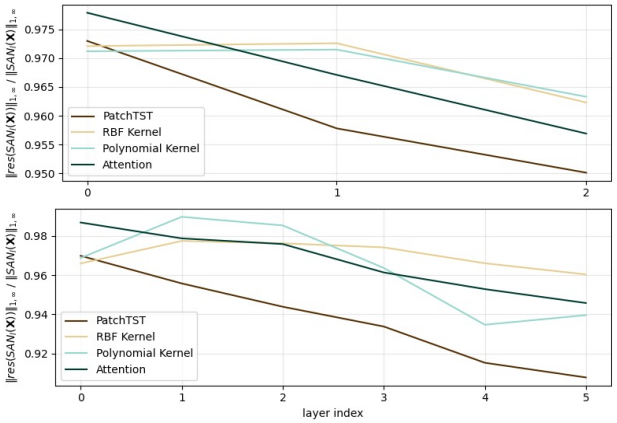

Figure 5. Relative norm of the residual along the depth for PatchTST, Attention, RBF kernel and polynomial kernel with different layers ([3, 6]) of transformer encoder on ETTh1.

6. Conclusion

The paper addresses the inherent nature of time series data, such as its low information density and the prevalence of distribution shifts and noises. By leveraging an attention mechanism tailored to time series, where the attention weights play a central role in representing data, we propose a novel and robust embedding strategy that utilizes global landmarks and a localized window to enrich the data representation. Our tailored attention map significantly outperforms the patching embedding-based SOTA transformer model in time series forecasting, a testament to its effectiveness. The results are compelling, with our approach yielding an average 3.6% improvement in MSE for SOTA multivariate time series prediction. The enhancement is designed to elevate predictive precision and introduces a modular component that is engineered for seamless integration within existing architectures, potentially reinforcing their resilience in generating embeddings from noisy signals.

Impact Statements

This paper presents work whose goal is to advance the field of Machine Learning. There are many potential societal consequences of our work, none which we feel must be specifically highlighted here.

References

Bao, H., Dong, L., Piao, S., and Wei, F. BEit: BERT pre-training of image transformers. In *International Conference on Learning Representations*, 2022.

Böse, J.-H., Flunkert, V., Gasthaus, J., Januschowski, T., Lange, D., Salinas, D., Schelter, S., Seeger, M., and Wang, Y. Probabilistic demand forecasting at scale. *Proceedings of the VLDB Endowment*, 10(12):1694–1705, 2017.

Box, G. E. and Jenkins, G. M. Some recent advances in forecasting and control. *Journal of the Royal Statistical Society. Series C (Applied Statistics)*, 17(2):91–109, 1968.

Box, G. E. and Pierce, D. A. Distribution of residual autocorrelations in autoregressive-integrated moving average time series models. *Journal of the American statistical Association*, 65(332):1509–1526, 1970.

Choromanski, K. M., Likhosherstov, V., Dohan, D., Song, X., Gane, A., Sarlos, T., Hawkins, P., Davis, J. Q., Mohiuddin, A., Kaiser, L., Belanger, D. B., Colwell, L. J., and Weller, A. Rethinking attention with performers. In *International Conference on Learning Representations*, 2021. URL https://openreview.net/forum?id=Ua6zuk0WRH.

Courty, P. and Li, H. Timing of seasonal sales. *The Journal of Business*, 72(4):545–572, 1999.

Devlin, J., Chang, M., Lee, K., and Toutanova, K. BERT: pre-training of deep bidirectional transformers for language understanding. In *Proceedings of the 2019 Conference of the North American Chapter of the Association for Computational Linguistics: Human Language Technologies (NAACL-HLT), Minneapolis, MN, USA, June 2-7, 2019*, pp. 4171–4186, 2019.

Dong, Y., Cordonnier, J.-B., and Loukas, A. Attention is not all you need: Pure attention loses rank doubly exponentially with depth. *ArXiv*, abs/2103.03404, 2021. URL https://api.semanticscholar.org/CorpusID:232134936.

Dosovitskiy, A., Beyer, L., Kolesnikov, A., Weissenborn, D., Zhai, X., Unterthiner, T., Dehghani, M., Minderer, M., Heigold, G., Gelly, S., Uszkoreit, J., and Houlsby, N. An image is worth 16x16 words: Transformers for image recognition at scale. In *9th International Conference on Learning Representations (ICLR), Austria, May 3-7, 2021*, 2021.

Ghojogh, B., Ghodsi, A., Karray, F., and Crowley, M. Reproducing kernel hilbert space, mercer's theorem, eigenfunctions, nyström method, and use of kernels in machine learning: Tutorial and survey. *ArXiv*, abs/2106.08443, 2021. URL https://api.semanticscholar.org/CorpusID:235446387.

Katharopoulos, A., Vyas, A., Pappas, N., and Fleuret, F. Transformers are rnns: Fast autoregressive transformers with linear attention. In *Proceedings of the International Conference on Machine Learning (ICML)*, 2020.

Kim, T., Kim, J., Tae, Y., Park, C., Choi, J.-H., and Choo, J. Reversible instance normalization for accurate time-series forecasting against distribution shift. In *International Conference on Learning Representations*, 2022.

Li, S., Jin, X., Xuan, Y., Zhou, X., Chen, W., Wang, Y.-X., and Yan, X. Enhancing the locality and breaking the memory bottleneck of transformer on time series forecasting. *arXiv preprint arXiv:1907.00235*, 2019.

Liu, Y., Hu, T., Zhang, H., Wu, H., Wang, S., Ma, L., and Long, M. itransformer: Inverted transformers are effective for time series forecasting. *arXiv preprint arXiv:2310.06625*, 2023.

Ma, X., Zhou, C., Kong, X., He, J., Gui, L., Neubig, G., May, J., and Zettlemoyer, L. Mega: Moving average equipped gated attention. In *The Eleventh International Conference on Learning Representations*, 2023. URL https://openreview.net/forum?id=qNLe3iq2El.

Mika, S., Schölkopf, B., Smola, A., Müller, K.-R., Scholz, M., and Rätsch, G. Kernel pca and de-noising in feature spaces. In Kearns, M., Solla, S., and Cohn, D. (eds.), *Advances in Neural Information Processing Systems*, volume 11. MIT Press, 1998. URL https://proceedings.neurips.cc/paper_files/paper/1998/file/226d1f15ecd35f784d2a20c3ecf56d7f-Paper.pdf.

Nie, Y., Nguyen, N. H., Sinthong, P., and Kalagnanam, J. A time series is worth 64 words: Long-term forecasting with transformers. *ArXiv*, abs/2211.14730, 2022.

Radford, A., Wu, J., Child, R., Luan, D., Amodei, D., and Sutskever, I. Language models are unsupervised multitask learners. 2019.

Song, K., Jung, Y., Kim, D., and Moon, I.-C. Implicit kernel attention. In *Proceedings of the AAAI Conference on Artificial Intelligence*, volume 35, pp. 9713–9721, 2021.

Tsai, Y.-H. H., Bai, S., Yamada, M., Morency, L.-P., and Salakhutdinov, R. Transformer dissection: An unified understanding for transformer's attention via the lens of kernel. In *Proceedings of the 2019 Conference on Empirical Methods in Natural Language Processing and the 9th International Joint Conference on Natural Language Processing (EMNLP-IJCNLP)*, pp. 4344–4353, 2019.

Vaswani, A. and etc. Attention is all you need. *arXiv preprint arXiv:1706.03762*, 2017.

Wen, Q., Yang, L., Zhou, T., and Sun, L. Robust time series analysis and applications: An industrial perspective. In *Proceedings of the 28th ACM SIGKDD Conference on Knowledge Discovery and Data Mining*, pp. 4836–4837, 2022.

Wen, Q., Zhou, T., Zhang, C., Chen, W., Ma, Z., Yan, J., and Sun, L. Transformers in time series: A survey. In *International Joint Conference on Artificial Intelligence(IJCAI)*, 2023.

Wilson, A. G., Hu, Z., Salakhutdinov, R., and Xing, E. P. Deep kernel learning. In *International Conference on Artificial Intelligence and Statistics*, 2015. URL https://api.semanticscholar.org/CorpusID:1443279.

Wu, H., Xu, J., Wang, J., and Long, M. Autoformer: Decomposition transformers with auto-correlation for long-term series forecasting. In *Advances in Neural Information Processing Systems (NeurIPS)*, pp. 101–112, 2021.

Wu, H., Hu, T., Liu, Y., Zhou, H., Wang, J., and Long, M. Timesnet: Temporal 2d-variation modeling for general time series analysis. In *The Eleventh International Conference on Learning Representations*, 2023. URL https://openreview.net/forum?id=ju_Uqw384Oq.

Xu, J., Wu, H., Wang, J., and Long, M. Anomaly transformer: Time series anomaly detection with association discrepancy. *arXiv preprint arXiv:2110.02642*, 2021.

Xue, W., Zhou, T., Wen, Q., Gao, J., Ding, B., and Jin, R. Make transformer great again for time series forecasting: Channel aligned robust dual transformer, 2023.

Yang, Y., Zhang, C., Zhou, T., Wen, Q., and Sun, L. Dcdetector: Dual attention contrastive representation learning for time series anomaly detection. *Proceedings of the 29th ACM SIGKDD Conference on Knowledge Discovery and Data Mining*, 2023. URL https://api.semanticscholar.org/CorpusID:259203116.

Zeng, A., Chen, M., Zhang, L., and Xu, Q. Are transformers effective for time series forecasting? 2023.

Zhou, H., Zhang, S., Peng, J., Zhang, S., Li, J., Xiong, H., and Zhang, W. Informer: Beyond efficient transformer for long sequence time-series forecasting. In *Proceedings of AAAI*, 2021.

Zhou, T., MA, Z., wang, x., Wen, Q., Sun, L., Yao, T., Yin, W., and Jin, R. Film: Frequency improved legendre memory model for long-term time series forecasting. In Koyejo, S., Mohamed, S., Agarwal, A., Belgrave, D., Cho, K., and Oh, A. (eds.), *Advances in Neural Information Processing Systems*, volume 35, pp. 12677–12690. Curran Associates, Inc., 2022a.

Zhou, T., Ma, Z., Wen, Q., Wang, X., Sun, L., and Jin, R. FEDformer: Frequency enhanced decomposed transformer for long-term series forecasting. In *Proc. 39th International Conference on Machine Learning (ICML 2022)*, 2022b.

Zhou, T., Niu, P., Wang, X., Sun, L., and Jin, R. One fits all: Power general time series analysis by pretrained LM. In *Thirty-seventh Conference on Neural Information Processing Systems*, 2023. URL https://openreview.net/forum?id=gMS6FVZvmF.

A. Full theoretical Analysis of attention as Robust Representation

In this section, we will show that using attention map as an alternative representation can be significantly more robust than the original inputs, particularly to the noise. In other words, attention map help reduce the impact of noises compared to the original inputs.

Let $x_i \in \mathbb{R}^d, i = 1, \ldots, n$ be n vectors. For simplicity of analysis, we assume that each vector is generated from one of $m < d$ Gaussian distributions, denoted by $\mathcal{N}(\mu_i, I_d), i = 1, \ldots, m$. For the convenience of analysis, we assume that $\langle \mu_i, \mu_j \rangle = \delta_{i,j} s$ for any $i, j \in [m]$. Let $n = mK$, and we choose to generate K vectors from each Gaussian distributions. In particular, vector x_{mj+i}, with $j = 0, \ldots, K-1, i = 1, \ldots, m$, is generated from Gaussian distribution $\mathcal{N}(\mu_i, I_d)$. Then, if we choose two vectors x_i^+ and x_j^+ that are sampled from the same Gaussian distribution, we have

$$\mathrm{E}[|x_i^+ - x_j^+|^2] = 2d$$

and if x_i^- and x_j^- are sampled from different distributions, we have

$$\mathrm{E}[|x_i^- - x_j^-|^2] = 2d + 2s$$

It is clearly that the relative difference between the two expected distance square is $O(s/d)$. In fact, we can further show that there is a significant chance for the distance between two data points sampled from the same distributions to be larger than the distance between two data points sampled from different distributions, implying that the added noises can significantly affect the geometrical relationship among the sampled data points. To this end, we write $x_i^+ = \mu_a + z_i^+$ and $x_j^+ = \mu_a + z_j^+$, where $z_i^+, z_j^+ \sim \mathcal{N}(0, I_d)$. Hence

$$|x_i^+ - x_j^+|^2 = |\underbrace{z_i^+ - z_j^+}_{:=u_+}|^2$$

It is clear that $|u_+|^2 \sim 2\chi_d^2$. In the meantime, by writing $x_i^- = \mu_b + z_i^-$ and $x_j^- = \mu_c + z_j^-$, with $z_i^-, z_j^- \sim \mathcal{N}(0, I_d)$, we have

$$|x_i^- - x_j^-|^2 = 2s + 2\underbrace{\langle \mu_b - \mu_c, z_i^- - z_j^- \rangle}_{:=v_-} + |\underbrace{z_i^- - z_j^-}_{:=u_-}|^2$$

It is clear that $v_- \sim \mathcal{N}(0, 2s)$ and $|u_-|^2 \sim 2\chi_d^2$. We want to bound the probability

$$\Pr\left(|u_-|^2 + 2v_- - |u_+|^2 \leq -2s\right)$$

First, using the standard concentration inequality for χ_d^2 distributions, we have

$$\Pr\left(\frac{1}{2}|u_-|^2 \leq d + 2\sqrt{d\delta} + 2\delta\right) \geq 1 - \exp(-\delta)$$

By setting $\delta = s^2/(16d)$, under the assumption $s^2 \leq 16d$, we have

$$\Pr\left(|u_-|^2 \leq 2d + s + \frac{s^2}{4d}\right) \geq 1 - \exp\left(-\frac{s^2}{16d}\right) \geq \frac{s^2}{32d}$$

Since $v_- \sim \mathcal{N}(0, 2s)$, we have

$$\Pr\left(v_- \geq \frac{2s}{3}\right) \leq \frac{3}{2\sqrt{2\pi}s} \exp\left(-\frac{s}{9}\right) \geq \frac{e^{-s/9}}{\sqrt{2}s}$$

and therefore

$$\Pr\left(|u_+|^2 + 2v_- \leq 2d + \frac{7s}{3} + \frac{s^2}{4d}\right) \leq \frac{s^2}{32d} - \frac{e^{-s/9}}{\sqrt{2}s}$$

In the meantime, we can also lower bound $|u_+|^2$. Using the fact the CDF for χ_2^2 is $1 - \exp(-x/2)$. We have

$$\Pr\left(|u_+|^2 \geq 2(1+\varepsilon)d\right) \geq \exp\left(-\frac{\varepsilon d}{2}\right)$$

By choosing $\varepsilon = 3s/(2d)$, we have

$$\Pr\left(|u_+|^2 \geq 2d + 3s\right) \geq \exp\left(-\frac{3s}{4}\right)$$

Combining the above two inequalities, we have

$$\Pr\left(|u_-|^2 - |u_+|^2 + 2v_- \leq -\frac{2s}{3} + \frac{s^2}{4d}\right) \geq \exp\left(-\frac{3s}{4}\right)\left(\frac{s^2}{32d} - \frac{e^{-s/9}}{\sqrt{2}s}\right)$$

when

$$s < d \leq \frac{\sqrt{2}s^3}{32}$$

we have

$$\Pr\left(|u_-|^2 - |u_+|^2 + 2v_- \leq -\frac{s}{3}\right) \geq \frac{1}{\sqrt{2}s}\exp\left(-\frac{3s}{4}\right)\left(1 - e^{-s/9}\right)$$

implying that there is a descent chance for $|x_i^- - x_j^-| < |x_i^+ - x_j^+|$.

Now, let's check the attention based representation, i.e. for any vector x, we represent it by $f(x)$ given below

$$f(x) = \left(\exp\left(\lambda\langle x, x_1\rangle\right), \ldots, \exp\left(\lambda\langle x, x_n\rangle\right)\right)$$

For simplicity, we sample a pair of data points $x_i^+, x_j^+ \sim \mathcal{N}(\mu_a, I_d)$ from the same distribution, and another pair of data points $x_i^- \sim \mathcal{N}(\mu_b, I_d)$ and $x_j^- \sim \mathcal{N}(\mu_c, I_d)$. We first represent each of these four data points by their attention map. We first compute the distance

$$\begin{aligned}
\mathrm{E}[|f(x_i^+) - f(x_j^+)|^2] &= \sum_{k=1}^{n} \mathrm{E}\left[\left|\exp\left(\lambda\langle x_i^+, x_k\rangle\right) - \exp\left(\lambda\langle x_j^+, x_k\rangle\right)\right|^2\right] \\
&= K\sum_{k=1}^{m} \mathrm{E}\left[\left|\exp\left(\lambda\langle x_i^+, x\rangle\right) - \exp\left(\lambda\langle x_j^+, x\rangle\right)\right|^2\right] \\
&= K\sum_{k=1}^{m} \mathrm{E}\left[2\exp\left(2\lambda\langle x_i^+, x\rangle\right) - 2\exp\left(\lambda\langle x, x_i^+ + x_j^+\rangle\right)\right]
\end{aligned}$$

To compute the above expectation, we first consider $k = a$. Define $z_i^+ = x_i^+ - \mu_a$, $z_j^+ = x_j^+ - \mu_a$, and $z = x - \mu_a$. We have

$$\begin{aligned}
&\mathrm{E}\left[2\exp\left(2\lambda\langle x_i^+, x\rangle\right) - 2\exp\left(\sqrt{2}\langle x, x_j^+\rangle\right)\right] \\
&= \mathrm{E}\left[2\exp\left(2\lambda(s + \langle z, z_i^+\rangle + \langle \mu_a, z_i^+ + z\rangle)\right) - 2\exp\left(\sqrt{2}\lambda\left(\sqrt{2}s + \langle z, z_j^+\rangle + \langle \mu_a, z_j^+ + z\rangle\right)\right)\right]
\end{aligned}$$

By taking the expectation over z_i^+ and z_j^+, given $\langle z_i^+, z+\mu_a\rangle \sim \mathcal{N}(0, |z+\mu_a|^2)$ and z_j^+ and $\langle z_j^+, z+\mu_a\rangle \sim \mathcal{N}(0, |z+\mu_a|^2)$, we have

$$\mathrm{E}_{z_i^+}\left[\exp\left(2\lambda\langle z_i^+, z + \mu_a\rangle\right)\right] = \exp\left(2\lambda^2|z+\mu_a|^2\right),\ \mathrm{E}_{z_j^+}\left[\exp\left(\sqrt{2}\lambda\langle z_j^+, z + \mu_a\rangle\right)\right] = \exp\left(\lambda^2|z+\mu_a|^2\right)$$

and therefore

$$\begin{aligned}
&\mathrm{E}\left[2\exp\left(2\lambda\langle x_i^+, x\rangle\right) - 2\exp\left(\sqrt{2}\langle x, x_j^-\rangle\right)\right] \\
&= \mathrm{E}\left[\exp\left(2\lambda\left(s + \langle \mu_a, z\rangle + \lambda|z+\mu_a|^2\right)\right)\right] - \mathrm{E}\left[\exp\left(\sqrt{2}\lambda\left(s + \langle \mu_a, z\rangle + \frac{\lambda}{\sqrt{2}}|z+\mu_a|^2\right)\right)\right]
\end{aligned}$$

Since

$$\begin{aligned}
&\mathrm{E}\left[\exp\left(2\lambda^2|z+\mu_a|^2+2\lambda\langle\mu_a,z\rangle\right)\right]\\
&= \frac{e^{2\lambda^2 s}}{(2\pi)^{d/2}}\int\exp\left(2\lambda^2|z|^2+2\lambda(2\lambda+1)\langle\mu_a,z\rangle-\frac{|z|^2}{2}\right)dz\\
&= \frac{e^{2\lambda^2 s}}{(2\pi)^{(d-1)/2}}\int\exp\left(-(1-4\lambda^2)\frac{|z_{d-1}|^2}{2}\right)dz_{d-1}\times\frac{1}{\sqrt{2\pi}}\int\exp\left(-(1-4\lambda^2)\frac{z^2}{2}+2\lambda(2\lambda+1)s^{1/2}z\right)\\
&= \frac{e^{2\lambda^2 s}}{(1-4\lambda^2)^{d/2}}\exp\left(\frac{2\lambda^2(1+2\lambda)^2 s}{1-4\lambda^2}\right)=\frac{e^{2\lambda^2 s}}{(1-4\lambda^2)^{d/2}}\exp\left(\frac{2\lambda^2(1+2\lambda)s}{1-2\lambda}\right):=C_1
\end{aligned}$$

and

$$\begin{aligned}
&\mathrm{E}\left[\exp\left(\sqrt{2}\lambda\langle\mu_a,z\rangle+\lambda^2|z+\mu_a|^2\right)\right]\\
&= \frac{e^{\lambda^2 s}}{(2\pi)^{d/2}}\int\exp\left(-(1-2\lambda^2)\frac{|z|^2}{2}+\lambda(\sqrt{2}+2\lambda)\langle z,\mu_a\rangle\right)dz\\
&= \frac{e^{\lambda^2 s}}{(1-2\lambda^2)^{d/2}}\exp\left(\frac{\lambda^2(1+\sqrt{2}\lambda)^2 s}{2(1-2\lambda^2)}\right)=\frac{e^{\lambda^2 s}}{(1-2\lambda^2)^{d/2}}\exp\left(\frac{\lambda^2(1+\sqrt{2}\lambda)s}{2(1-\sqrt{2}\lambda)}\right):=C_2
\end{aligned}$$

we have

$$\begin{aligned}
&\mathrm{E}\left[2\exp\left(2\lambda\langle x_i^+,x\rangle\right)-2\exp\left(\langle x,x_i^++x_j^+\rangle\right)\right]\\
&= \frac{2e^{2\lambda(1+\lambda)s}}{(1-4\lambda^2)^{d/2}}\exp\left(\frac{2\lambda^2(1+2\lambda)s}{1-2\lambda}\right)-\frac{2e^{\lambda(2+\lambda)s}}{(1-2\lambda^2)^{d/2}}\exp\left(\frac{\lambda^2(1+\sqrt{2}\lambda)s}{2(1-\sqrt{2}\lambda)}\right)
\end{aligned}$$

For $k\neq a$, we have

$$\begin{aligned}
&\mathrm{E}\left[2\lambda\exp\left(2\lambda\langle x_i^+,x\rangle\right)-2\exp\left(\sqrt{2}\langle x,x_j^+\rangle\right)\right]\\
&= \frac{2e^{2\lambda^2 s}}{(1-4\lambda^2)^{d/2}}\exp\left(\frac{2\lambda^2(1+2\lambda)s}{1-2\lambda}\right)-\frac{2e^{\lambda^2 s}}{(1-2\lambda^2)^{d/2}}\exp\left(\frac{\lambda^2(1+\sqrt{2}\lambda)s}{2(1-\sqrt{2}\lambda)}\right)
\end{aligned}$$

By combining the above results, we have

$$\mathrm{E}\left[\left|f(x_i^+)-f(x_j^+)\right|^2\right]=2K\left(e^{2\lambda s}+m-1\right)(C_1-C_2)$$

We then compute the distance between $f(x_i^-)$ and $f(x_j^-)$, which is given by

$$\mathrm{E}\left[|f(x_i^-)-f(x_j^-)|^2\right]=K\sum_{k=1}^{m}\mathrm{E}\left[\exp\left(2\lambda\langle x_i^-,x\rangle\right)+\exp\left(2\lambda\langle x_j^-,x\rangle\right)-2\exp\left(\lambda\langle x,x_i^-+x_j^-\rangle\right)\right]$$

First, for the case $k=b$, we have

$$\begin{aligned}
&\mathrm{E}\left[\exp\left(2\lambda\langle x_i^+,x\rangle\right)+\exp\left(2\lambda\langle x_j^+,x\rangle\right)-2\exp\left(\lambda\langle x,x_i^++x_j^+\rangle\right)\right]\\
&= \mathrm{E}\left[\exp\left(2\lambda s+2\lambda\langle\mu_b,z+z_i^-\rangle+2\lambda\langle z,z_i^-\rangle\right)+\exp\left(2\langle\mu_b,z\rangle+2\lambda\langle\mu_c,z_i^-\rangle+2\lambda\langle z,z_i^-\rangle\right)\right]\\
&\quad -2\mathrm{E}\left[\exp\left(\lambda s+\lambda\langle\mu_b,z_i^-+z_j^-\rangle+\lambda\langle\mu_b+\mu_c,z_j\rangle+\lambda\langle z,z_i^-+z_j^-\rangle\right)\right]\\
&= \mathrm{E}\left[\exp\left(2\lambda s+2\lambda^2|z+\mu_b|^2+2\lambda\langle\mu_b,z\rangle\right)\right]+\mathrm{E}\left[\exp\left(2\lambda\langle\mu_b,z\rangle+2\lambda^2|\mu_c+z|^2\right)\right]\\
&\quad -2\mathrm{E}\left[\exp\left(\lambda s+\lambda\langle\mu_b+\mu_c,z_j^-\rangle+\frac{\lambda^2|z_i^-+z_j^-|^2}{2}\right)\right]\\
&= e^{2\lambda s}C_1+\mathrm{E}\left[\exp\left(2\lambda^2 s+2\lambda\langle\mu_b+2\lambda\mu_c,z\rangle+2\lambda^2|z|^2\right)\right]-2\mathrm{E}\left[\exp\left(\lambda s+\lambda\langle\mu_b+\mu_c,z_j^-\rangle+\lambda^2|z_i^-|^2\right)\right]\\
&= e^{2\lambda s}C_1+\frac{e^{2\lambda^2 s}}{(1-4\lambda^2)^{d/2}}\exp\left(\frac{2\lambda^2(1+4\lambda^2)s}{1-4\lambda^2}\right)-\frac{2e^{\lambda s+\lambda^2 s}}{(1-2\lambda^2)^{d/2}}\\
&\geq \left(e^{2\lambda s}+e^{-8\lambda^3}\right)C_1-2\exp\left(-\frac{\lambda^2 s}{2}\right)C_2
\end{aligned}$$

Second, for $k \neq b$ and $k \neq c$, we have

$$\begin{aligned}
&\mathrm{E}\left[\exp\left(2\lambda\langle x_i^+, x\rangle\right) + \exp\left(2\lambda\langle x_j^+, x\rangle\right) - 2\exp\left(\lambda\langle x, x_i^+ + x_j^+\rangle\right)\right] \\
&= 2\mathrm{E}\left[\exp\left(2\langle\mu_b, z\rangle + 2\lambda\langle\mu_c, z_i^-\rangle + 2\lambda\langle z, z_i^-\rangle\right)\right] \\
&\quad -2\mathrm{E}\left[\exp\left(\lambda\langle\mu_k, z_i^- + z_j^-\rangle + \lambda\langle\mu_b + \mu_c, z_j\rangle + \lambda\langle z, z_i^- + z_j^-\rangle\right)\right] \\
&= 2\mathrm{E}\left[\exp\left(2\lambda\langle\mu_b, z\rangle + 2\lambda^2|\mu_c + z|^2\right)\right] - 2\mathrm{E}\left[\exp\left(\sqrt{2}\lambda\langle\mu_k + z, z_i^-\rangle + \lambda\langle\mu_b + \mu_c, z_j^-\rangle\right)\right] \\
&= 2\mathrm{E}\left[\exp\left(2\lambda^2 s + 2\lambda\langle\mu_b + 2\lambda\mu_c, z\rangle + 2\lambda^2|z|^2\right)\right] - 2\mathrm{E}\left[\exp\left(\lambda^2 s + \lambda^2|\mu_k + z|^2\right)\right] \\
&= \frac{2e^{2\lambda^2 s}}{(1-4\lambda^2)^{d/2}}\exp\left(\frac{2\lambda^2(1+4\lambda^2)}{1-4\lambda^2}\right) - \frac{2e^{\lambda^2 s}}{(1-2\lambda^2)^{d/2}} \\
&\geq 2e^{-8\lambda^3}C_1 - 2\exp\left(-\frac{\lambda^2 s}{2}\right)C_2
\end{aligned}$$

Thus, we have

$$\mathrm{E}\left[|f(x_i^-) - f(x_j^-)|^2\right] \geq K\left(2\left(e^{2\lambda s} + me^{-8\lambda^3}\right)C_1 - m\exp\left(-\frac{\lambda^2 s}{2}\right)C_2\right) \geq 2Ke^{2\lambda s}C_1$$

and hence

$$\frac{\mathrm{E}\left[|f(x_i^-) - f(x_i^-)|^2\right] - \mathrm{E}\left[|f(x_i^+) - f(x_i^+)|^2\right]}{\mathrm{E}\left[|f(x_i^+) - f(x_i^+)|^2\right]} \geq \frac{C_1/(C_1 - C_2) - \left(1 + (m-1)e^{-2\lambda s}\right)}{1 + (m-1)e^{-2\lambda s}}$$

Since

$$\frac{C_1}{C_1 - C_2} = \frac{1}{1 - \underbrace{e^{-\lambda^2 s}\left(\frac{1-4\lambda^2}{1-2\lambda^2}\right)^{d/2}\exp\left(\lambda^2 s\left[\frac{1+\sqrt{2}\lambda}{2(1-\sqrt{2}\lambda)} - \frac{2(1+2\lambda)}{1-2\lambda}\right]\right)}_{:=\Gamma}}$$

It is easy to verify that when $\lambda^2 = 1/d$, $\Gamma = \Omega(1)$, and by further assuming that s is sufficiently large that $e^{-2\lambda s} \leq \gamma/(2(m-1))$, we have

$$\frac{\mathrm{E}\left[|f(x_i^-) - f(x_i^-)|^2\right] - \mathrm{E}\left[|f(x_i^+) - f(x_i^+)|^2\right]}{\mathrm{E}\left[|f(x_i^+) - f(x_i^+)|^2\right]} \geq \frac{\Gamma}{2+\Gamma} \geq \frac{\Gamma}{3}$$

This analysis shows that by using attention as a representation, we are able to easily distinguish if data points come from the same distribution, even with a very large noise, which become difficult if we use the original inputs.

B. Detailed Results

B.1. Detailed Results of Multivariate Forecasting

B.2. Detailed Results of Multivariate Forecasting with RBF Kernel and Polynomial Kernel

B.3. Detailed Results of Utilize AttnEmbed as A Plug-in

B.4. Detailed Results of Utilize AttnEmbed as A Plug-in

Table 5. Multivariate forecasting results. The lookback length is set as 96. All models are evaluated on 4 different prediction horizons {96, 192, 336, 720}. A lower MSE indicates better performance. The best ones are in Bold, and the second ones are underlined.

Methods		**AttnEmbed**		PatchTST		TimesNet		DLinear		FiLM		FEDformer		Autoformer		Informer	
Metric		MSE	MAE	MSE	MAE	MSE	MAE	MSE	MAE	MSE	MAE	MSE	MAE	MSE	MAE	MSE	MAE
Weather	96	**0.171**	**0.215**	0.178	0.219	0.172	0.220	0.196	0.255	0.193	0.234	0.217	0.296	0.266	0.336	0.300	0.384
	192	**0.218**	**0.257**	0.224	0.259	0.219	0.261	0.237	0.296	0.236	0.269	0.276	0.336	0.307	0.367	0.598	0.544
	336	**0.274**	**0.297**	0.278	0.298	0.280	0.306	0.283	0.335	0.288	0.304	0.339	0.380	0.359	0.395	0.578	0.523
	720	0.348	**0.346**	0.350	**0.346**	0.365	0.359	**0.345**	0.381	0.358	0.350	0.403	0.428	0.419	0.428	1.059	0.741
	Avg	**0.252**	**0.278**	0.257	0.280	0.259	0.287	0.265	0.317	0.269	0.339	0.309	0.360	0.338	0.382	0.634	0.548
ETTh1	96	**0.367**	**0.398**	0.393	0.408	0.384	0.402	0.386	0.400	0.388	0.401	0.376	0.419	0.449	0.459	0.865	0.713
	192	**0.420**	**0.428**	0.445	0.434	0.436	0.429	0.437	0.432	0.443	0.439	**0.420**	0.448	0.500	0.482	1.008	0.792
	336	**0.448**	**0.438**	0.484	0.451	0.491	0.469	0.481	0.459	0.488	0.466	0.459	0.465	0.521	0.496	1.107	0.809
	720	**0.454**	**0.459**	0.480	0.471	0.521	0.500	0.519	0.516	0.525	0.519	0.506	0.507	0.514	0.512	1.181	0.865
	Avg	**0.422**	**0.430**	0.450	0.440	0.458	0.450	0.456	0.452	0.461	0.456	0.440	0.460	0.496	0.487	1.040	0.795
ETTh2	96	0.296	0.346	**0.294**	**0.343**	0.340	0.374	0.333	0.387	0.296	0.344	0.358	0.397	0.346	0.388	3.755	1.525
	192	**0.369**	**0.392**	0.377	0.393	0.402	0.414	0.477	0.476	0.389	0.402	0.429	0.439	0.456	0.452	5.602	1.931
	336	**0.376**	**0.405**	0.381	0.409	0.452	0.452	0.594	0.541	0.418	0.430	0.496	0.487	0.482	0.486	4.721	1.835
	720	**0.405**	**0.432**	0.412	0.471	0.462	0.468	0.831	0.657	0.433	0.448	0.463	0.474	0.515	0.511	3.647	1.625
	Avg	**0.361**	**0.393**	0.366	0.404	0.414	0.427	0.559	0.515	0.384	0.406	0.437	0.449	0.450	0.459	4.431	1.729
ETTm1	96	**0.317**	**0.356**	0.321	0.360	0.338	0.375	0.345	0.372	0.348	0.367	0.379	0.416	0.505	0.475	0.672	0.571
	192	**0.357**	**0.381**	0.362	0.384	0.371	0.387	0.380	0.389	0.387	0.385	0.426	0.441	0.553	0.496	0.795	0.669
	336	**0.387**	0.404	0.392	**0.402**	0.410	0.411	0.413	0.413	0.418	0.405	0.445	0.459	0.621	0.537	1.212	0.871
	720	**0.448**	0.439	0.450	**0.435**	0.478	0.450	0.474	0.453	0.479	0.440	0.543	0.490	0.671	0.561	1.166	0.823
	Avg	**0.377**	**0.395**	0.381	**0.395**	0.400	0.406	0.403	0.407	0.408	0.399	0.448	0.452	0.588	0.517	0.961	0.734
ETTm2	96	0.181	0.265	**0.178**	**0.260**	0.187	0.267	0.193	0.292	0.183	0.266	0.203	0.287	0.255	0.339	0.365	0.453
	192	**0.245**	**0.304**	0.249	0.307	0.249	0.309	0.284	0.362	0.247	0.305	0.269	0.328	0.281	0.340	0.533	0.563
	336	**0.309**	0.349	0.313	0.346	0.321	0.351	0.369	0.427	**0.309**	**0.343**	0.325	0.366	0.339	0.372	1.363	0.887
	720	0.409	0.407	**0.400**	**0.398**	0.408	0.403	0.554	0.522	0.407	**0.398**	0.421	0.415	0.433	0.432	3.379	1.338
	Avg	0.286	0.331	**0.285**	**0.327**	0.291	0.333	0.350	0.401	0.287	0.328	0.305	0.349	0.327	0.371	1.410	0.810
ECL	96	**0.166**	**0.252**	0.174	0.259	0.168	0.272	0.197	0.282	0.198	0.276	0.193	0.308	0.201	0.317	0.274	0.368
	192	**0.172**	**0.259**	0.178	0.265	0.184	0.289	0.196	0.285	0.198	0.279	0.201	0.315	0.222	0.334	0.296	0.386
	336	**0.191**	**0.277**	0.196	0.282	0.198	0.300	0.209	0.301	0.217	0.301	0.214	0.329	0.254	0.361	0.300	0.394
	720	0.231	**0.309**	0.237	0.316	**0.220**	0.320	0.245	0.333	0.279	0.357	0.246	0.355	0.254	0.361	0.373	0.439
	Avg	**0.189**	**0.274**	0.196	0.280	0.192	0.295	0.212	0.300	0.223	0.303	0.214	0.327	0.227	0.338	0.311	0.397
Traffic	96	**0.428**	**0.276**	0.477	0.305	0.593	0.321	0.650	0.396	0.649	0.391	0.587	0.366	0.613	0.388	0.274	0.368
	192	**0.434**	**0.274**	0.471	0.299	0.617	0.336	0.598	0.370	0.603	0.366	0.604	0.373	0.616	0.382	0.296	0.386
	336	**0.448**	**0.282**	0.485	0.305	0.629	0.336	0.605	0.373	0.613	0.371	0.621	0.383	0.622	0.337	0.300	0.394
	720	**0.478**	**0.299**	0.518	0.325	0.640	0.350	0.645	0.394	0.692	0.427	0.626	0.382	0.660	0.408	0.373	0.439
	Avg	**0.447**	**0.282**	0.487	0.308	0.620	0.336	0.625	0.383	0.639	0.389	0.610	0.376	0.628	0.379	0.311	0.397

Table 6. Multivairate forecasting results with RBF kernel and polynomial kernel. The lookback length is set as 96. All models are evaluated on 4 different prediction horizons {96, 192, 336, 720}. A lower MSE indicates better performance. The best ones are in Bold, and the second ones are underlined.

Methods		AttnEmbed		RBF Kernel		Polynomial Kernel		PatchTST		TimesNet	
Metric		MSE	MAE	MSE	MAE	MSE	MAE	MSE	MAE	MSE	MAE
Weather	96	**0.171**	**0.215**	0.175	0.220	0.174	0.216	0.178	0.219	0.172	0.220
	192	**0.218**	**0.257**	0.222	0.258	0.221	**0.257**	0.224	0.259	0.219	0.261
	336	0.274	0.297	0.276	0.297	**0.272**	**0.296**	0.278	0.298	0.280	0.306
	720	0.348	**0.346**	**0.347**	**0.346**	0.350	**0.346**	0.350	**0.346**	0.365	0.359
	Avg	**0.252**	**0.278**	0.255	0.280	0.254	0.279	0.257	0.280	0.259	0.287
ETTh1	96	**0.367**	**0.398**	0.374	**0.398**	0.380	0.400	0.393	0.408	0.384	0.402
	192	**0.420**	**0.428**	0.441	0.436	0.437	0.431	0.445	0.434	0.436	0.429
	336	**0.448**	**0.438**	0.475	0.452	0.457	0.442	0.484	0.451	0.491	0.469
	720	0.454	0.459	0.491	0.472	**0.450**	**0.453**	0.480	0.471	0.521	0.500
	Avg	**0.422**	**0.430**	0.445	0.439	0.431	0.431	0.450	0.440	0.458	0.450
ETTm1	96	0.317	0.356	**0.316**	0.356	0.318	**0.355**	0.321	0.360	0.338	0.375
	192	0.357	0.381	0.358	0.380	**0.354**	**0.377**	0.362	0.384	0.371	0.387
	336	**0.387**	0.404	0.389	0.403	0.391	0.403	0.392	**0.402**	0.410	0.411
	720	**0.448**	0.439	0.450	**0.435**	0.453	0.437	0.450	**0.435**	0.478	0.450
	Avg	**0.377**	0.395	0.378	**0.393**	0.379	**0.393**	0.381	0.395	0.400	0.406

Table 7. Utilize AttnEmbed as a plug-in. The lookback length is 336 for PatchTST and 96 for CARD. All models are evaluated on 4 different prediction horizons {96, 192, 336, 720}. A lower MSE indicates better performance.

Methods		PatchTST(42)		PatchTST(42) +AttnEmbed		CARD		CARD +AttnEmbed	
Metric		MSE	MAE	MSE	MAE	MSE	MAE	MSE	MAE
Weather	96	0.152	0.199	**0.151**	**0.199**	**0.150**	**0.188**	0.152	0.190
	192	0.197	0.243	**0.195**	**0.240**	0.202	0.238	**0.200**	**0.237**
	336	0.249	0.283	**0.246**	**0.282**	0.260	0.282	**0.259**	**0.282**
	720	0.320	0.335	**0.320**	**0.331**	0.343	0.353	**0.341**	**0.334**
	Avg	0.229	0.265	**0.227**	**0.263**	0.239	0.265	**0.238**	**0.260**
ETTh1	96	0.375	0.399	**0.374**	**0.397**	0.383	0.391	**0.379**	**0.390**
	192	0.414	0.421	**0.412**	**0.423**	0.435	0.420	**0.428**	**0.421**
	336	0.431	0.436	**0.420**	**0.432**	0.479	0.442	**0.472**	**0.440**
	720	0.449	0.466	**0.430**	**0.455**	0.471	0.461	**0.469**	**0.459**
	Avg	0.417	0.430	**0.409**	**0.426**	0.442	0.428	**0.436**	**0.427**
ETTm1	96	0.290	0.342	**0.286**	**0.341**	0.319	0.347	**0.316**	**0.344**
	192	0.332	0.369	**0.331**	**0.369**	0.363	0.370	**0.356**	**0.365**
	336	0.366	0.392	**0.363**	**0.390**	0.392	0.390	**0.386**	**0.386**
	720	0.420	0.424	**0.410**	**0.416**	0.458	0.425	**0.450**	**0.422**
	Avg	0.352	0.381	**0.347**	**0.379**	0.383	0.384	**0.377**	**0.379**

Table 8. Ablation on EMA and landmark. The lookback length is 96. All models are evaluated on 4 different prediction horizons {96, 192, 336, 720}. A lower MSE indicates better performance.

Methods		AttnEmbed		AttnEmbed w/o EMA		AttnEmbed w/o Landmark	
Metric		MSE	MAE	MSE	MAE	MSE	MAE
ETTh1	96	0.367	0.398	0.378	0.398	0.370	0.400
	192	0.420	0.428	0.423	0.425	0.421	0.427
	336	0.448	0.438	0.456	0.430	0.440	0.436
	720	0.454	0.459	0.472	0.455	0.461	0.454
	Avg	0.422	0.430	0.432	0.427	0.423	0.429
ETTm1	96	0.317	0.356	0.319	0.360	0.326	0.365
	192	0.357	0.381	0.374	0.391	0.370	0.384
	336	0.387	0.404	0.396	0.402	0.396	0.403
	720	0.448	0.439	0.449	0.437	0.455	0.436
	Avg	0.377	0.395	0.384	0.397	0.386	0.397